Fuzzy LQG with high-gain observer for robust control of a double inverted pendulum on a cart

Thi-Van-Anh NGUYEN[1], Van-Hoan TRAN[1], Doan-Khai TA[1] and Manh-Linh NGUYEN[1,*]

[1] *School of Electrical and Electronic Engineering, Hanoi University of Science and Technology*
[*] *Corresponding author E-mail: linh.nguyenmanh@hust.edu.vn*
DOI: https://doi.org/10.64032/mca.v30i1.385

Abstract

This paper addresses the stabilization problem of the double inverted pendulum on a cart, a benchmark system that exhibits strong nonlinearity and instability. To enhance control performance under realistic operating conditions, two hybrid control schemes are proposed: the fuzzy linear quadratic regulator and the fuzzy linear quadratic gaussian controller. The former strategy is constructed by integrating fuzzy logic with a classical linear quadratic regulator framework to improve adaptability and dynamic response. At the same time, the latter strategy extends this approach by incorporating a Kalman filter for robust state estimation in noisy environments. Furthermore, a high-gain observer is developed to estimate unmeasurable velocity states using only position and angular measurements, thereby reducing the dependency on full-state sensing. Simulation studies are conducted for both the ideal case, with complete and noise-free measurements, and the realistic case, involving measurement noise and external disturbances. The results demonstrate that the proposed fuzzy linear quadratic gaussian controller with observer consistently outperforms its counterpart - the fuzzy linear quadratic regulator, and achieves superior robustness.

Keywords: *Double Inverted Pendulum on a Cart; Fuzzy Linear Quadratic Gaussian; High-Gain Observer; Kalman Filter; Robust Control*

1. Introduction

The control of underactuated systems remains one of the most challenging research topics in control engineering and robotics [1]. Among typical systems such as two-degree-of-freedom pendulum systems [2], [3] or inverted pendulum-on-cart systems [4], the double inverted pendulum on a cart (DIPC) has been extensively investigated as a benchmark problem due to its rich dynamics and practical relevance. The DIPC exhibits strong nonlinear behavior, multivariable coupling, and inherently unstable equilibrium points, making it an ideal testbed for evaluating and comparing advanced control algorithms. Beyond its theoretical appeal, the DIPC also has practical significance since its dynamic characteristics are analogous to many engineering applications, such as robotic manipulators [5], walking robots [6], self-balancing vehicles [7], and aerospace systems [8]. Therefore, designing effective controllers for the DIPC not only contributes to academic research but also provides valuable insights into the control of complex real-world systems.

Over the years, a wide range of control methods have been applied to the DIPC, including classical approaches such as the Linear Quadratic Regulator (LQR) and the Linear Quadratic Gaussian (LQG) controller. These controllers are attractive because they are grounded in optimal control theory and provide systematic procedures for balancing performance and control effort. However, their performance is often limited when applied to nonlinear systems or under conditions where the model is uncertain, and disturbances are present. For example, the standard LQR relies on the availability of complete and accurate state information, which is often impractical in real-world scenarios. Likewise, LQG controllers combine the Kalman Filter [9] with LQR to handle noise, but they still assume linear system behavior, which restricts their effectiveness when faced with strong nonlinearities. To address these shortcomings, researchers have introduced a variety of advanced strategies, including adaptive control, sliding mode control, neural-network-based control, and model predictive control. While these methods improve robustness and adaptability, they can be computationally demanding or difficult to implement in real-time applications. Even though, compared with other underactuated systems such as the inverted pendulum or overhead crane, which have been extensively studied in various aspects including hierarchical sliding mode control [10], optimal control [11], robust control techniques [12], and fault-tolerant control [13], the methods to enhance the performance of the DIPC remain quite limited.

In this context, fuzzy logic–based methods [14] have emerged as a promising solution for controlling nonlinear and uncertain systems such as the DIPC. Fuzzy controllers exploit linguistic rules and membership functions to approximate nonlinear mappings without requiring an exact mathematical model. By combining fuzzy logic with classical control frameworks such as Lyapunov theory and Linear Matrix Inequalities (LMIs) [15], hybrid strategies can be developed that inherit the strengths of both approaches [16]. Not only that, the exploitation of fuzzy logic has been developed to represent different dynamic models of nonlinear systems, including state-space models [16], fractional-order systems [17], and descriptor models [12], [18], by using the Takagi–Sugeno fuzzy model. Obviously, the advantages of fuzzy logic in control design have been explicitly demonstrated. However, the complexity remains the largest barrier to applying the aforementioned methods to experiments. A simpler way to achieve robustness while re-

Received: 13 October 2025; Revised: 17 November 2025; Accepted: 21 November 2025.

ducing complexity is to combine fuzzy logic with LQR design. One such example is the Fuzzy Linear Quadratic Regulator (FLQR) [19], which integrates fuzzy inference with the LQR design. This hybrid controller enhances adaptability, provides smoother control actions, and improves robustness against parameter variations and modeling uncertainties. However, despite these advantages, challenges remain. When system states cannot be measured directly or when sensor signals are corrupted by noise, the FLQR controller cannot achieve its full potential. Existing studies have often assumed ideal measurement conditions, which limit the applicability of these methods to practical engineering problems. Therefore, there is a need for a more comprehensive solution that addresses both the nonlinear characteristics of the DIPC and the practical constraints of noisy and incomplete state measurements.

To overcome these challenges, this paper proposes a new control framework that combines fuzzy logic, optimal control, and advanced state estimation techniques. Specifically, an FLQG controller is developed by integrating the Kalman Filter into the FLQR structure. The Kalman Filter provides robust estimation of unmeasured or noisy states, enabling the controller to function effectively even in the presence of measurement disturbances. In addition, a high-gain observer (HGO) [20] is incorporated to estimate unmeasured velocity states based solely on measurable variables such as cart position and pendulum angles. The HGO is particularly attractive because of its simple structure, fast convergence, and ease of implementation in both simulations and real-time applications. By combining the FLQG controller with the HGO, the proposed method addresses the dual challenges of system nonlinearity and measurement noise. This integrated approach aims to improve stability, robustness, and accuracy in the stabilization of the DIPC under both idealized and realistic operating conditions.

2. Modeling

The DIPC considered in this study is shown in Fig. 1. The cart translates along a horizontal track with position denoted by θ_0. Two rigid links are connected in series: the first pendulum is hinged to the cart and rotates with respect to the vertical by angle θ_1, while the second pendulum is attached to the tip of the first and forms angle θ_2 with the vertical. This configuration is a classical underactuated, strongly nonlinear benchmark widely used to assess advanced control methods.

The cart has mass $m_0 = 0.8$ kg. The first and second pendulums have masses $m_1 = 0.5$ kg and $m_2 = 0.3$ kg, lengths $L_1 = 0.3$ m and $L_2 = 0.2$ m, and moments of inertia $J_1 = 0.015\ \mathrm{kg}\cdot\mathrm{m}^2$ and $J_2 = 0.009\ \mathrm{kg}\cdot\mathrm{m}^2$, respectively. The lengths $l_1 = L_1/2 = 0.15$ m and $l_2 = L_2/2 = 0.1$ m. The gravitational acceleration is $g = 9.8\ \mathrm{m/s}^2$. These parameters are employed in the subsequent Lagrangian formulation and the derivation of the system dynamics. Applying the Lagrange equation, the dynamic model of the system is obtained as follows:

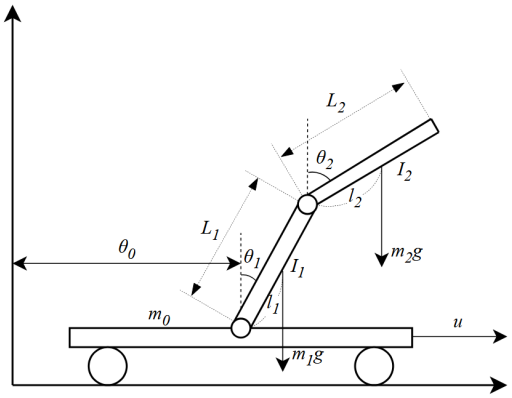

Figure 1: Double inverted pendulum on a cart model.

$$\frac{d}{dt}\left(\frac{\partial L}{\partial \dot{\theta}}\right) - \frac{\partial L}{\partial \theta} = Q. \tag{1}$$

The generalized coordinate vector is defined as $\theta = \begin{bmatrix}\theta_0 & \theta_1 & \theta_2 & \dot{\theta}_0 & \dot{\theta}_1 & \dot{\theta}_2\end{bmatrix}^T$, with the generalized force vector given by $Q = \begin{bmatrix}u & 0 & 0\end{bmatrix}^T$. The variables θ_i and $\dot{\theta}_i$, where $i \in \{0,1,2\}$, denote the angular displacements and angular velocities, respectively. The Lagrangian of the system is expressed as $L = T - P$, where T_i represents the kinetic energy and P_i the potential energy of each component ($i = 0,1,2$), while Q accounts for the generalized forces or torques acting on the joints.

$$T = T_0 + T_1 + T_2, \quad P = P_0 + P_1 + P_2.$$

The kinetic energies of the cart, the first pendulum, and the second pendulum are determined, where the energy of each pendulum consists of both translational and rotational components.

$$\begin{aligned}
T_0 &= \frac{1}{2} m_0 \dot{\theta}_0^2 \\
T_1 &= \frac{1}{2} m_1 \left[\left(\dot{\theta}_0 + l_1 \dot{\theta}_1 \cos\theta_1\right)^2 + \left(l_1 \dot{\theta}_1 \sin\theta_1\right)^2 \right] + \frac{1}{2} J_1 \dot{\theta}_1^2 \\
T_2 &= \frac{1}{2} m_2 \Big[\left(\dot{\theta}_0 + L_1 \dot{\theta}_1 \cos\theta_1 + l_2 \dot{\theta}_2 \cos\theta_2\right)^2 \\
&\quad + \left(L_1 \dot{\theta}_1 \sin\theta_1 + l_2 \dot{\theta}_2 \sin\theta_2\right)^2 \Big] + \frac{1}{2} J_2 \dot{\theta}_2^2
\end{aligned}$$

The potential energies are given by:

$$P_0 = 0, \quad P_1 = m_1 g l_1 \cos\theta_1, \quad P_2 = m_2 g (L_1 \cos\theta_1 + l_2 \cos\theta_2)$$

Accordingly, the Lagrangian function can be written as:

$$\begin{aligned}
L = {} & \frac{1}{2}(m_0 + m_1 + m_2)\dot{\theta}_0^2 + \frac{1}{2}(m_1 l_1^2 + J_1 + m_2 L_1^2)\dot{\theta}_1^2 \\
& + \frac{1}{2}(m_2 l_2^2 + J_2)\dot{\theta}_2^2 + (m_1 l_1 + m_2 L_1)\cos\theta_1 \dot{\theta}_0 \dot{\theta}_1 \\
& + m_2 l_2 \cos\theta_2 \dot{\theta}_0 \dot{\theta}_2 + m_2 L_1 l_2 \cos(\theta_1 - \theta_2)\dot{\theta}_1 \dot{\theta}_2 \\
& - (m_1 l_1 + m_2 L_1) g \cos\theta_1 - m_2 l_2 g \cos\theta_2.
\end{aligned} \tag{2}$$

The equations of motion derived from the Lagrange formulation are:

$$\begin{aligned}
&\frac{d}{dt}\left(\frac{\partial L}{\partial \dot{\theta}_0}\right) - \frac{\partial L}{\partial \theta_0} = u, \\
&\frac{d}{dt}\left(\frac{\partial L}{\partial \dot{\theta}_1}\right) - \frac{\partial L}{\partial \theta_1} = 0, \\
&\frac{d}{dt}\left(\frac{\partial L}{\partial \dot{\theta}_2}\right) - \frac{\partial L}{\partial \theta_2} = 0.
\end{aligned} \tag{3}$$

Consequently, the dynamic equations of the DIPC can be written as:

$$u = (m_0+m_1+m_2)\ddot{\theta}_0 + (m_1l_1+m_2L_1)\cos\theta_1\ddot{\theta}_1 + m_2l_2\cos\theta_2\ddot{\theta}_2 - (m_1l_1+m_2L_1)\sin\theta_1\dot{\theta}_1^2 \quad (4)$$

$$- m_2l_2\sin\theta_2\dot{\theta}_2^2, \quad (5)$$

$$0 = (m_1l_1+m_2L_1)\ddot{\theta}_0 \quad (6)$$

$$+ (m_1l_1^2+J_1+m_2L_1^2)\ddot{\theta}_1 + m_2L_1l_2\cos(\theta_1-\theta_2)\ddot{\theta}_2 + m_2L_1l_2\sin(\theta_1-\theta_2)\dot{\theta}_2^2 - (m_1l_1+m_2L_1)g\sin\theta_1, \quad (7)$$

$$0 = m_2l_2\cos\theta_2\ddot{\theta}_0 + m_2L_1l_2\cos(\theta_1-\theta_2)\ddot{\theta}_1 + (m_2l_2^2+J_2)\ddot{\theta}_2 - m_2L_1l_2\sin(\theta_1-\theta_2)\dot{\theta}_1^2 - m_2l_2g\sin\theta_2. \quad (8)$$

The dynamic equations can be written in matrix form as:

$$\mathbf{D}(\theta)\ddot{\theta} + \mathbf{C}(\theta,\dot{\theta})\dot{\theta} + \mathbf{G}(\theta) = \mathbf{H}u \quad (9)$$

where:

$$\mathbf{D}(\theta) = \begin{bmatrix} b_1 & b_2\cos\theta_1 & b_3\cos\theta_2 \\ b_2\cos\theta_1 & b_4 & b_5\cos(\theta_1-\theta_2) \\ b_3\cos\theta_2 & b_5\cos(\theta_1-\theta_2) & b_6 \end{bmatrix},$$

$$\mathbf{C}(\theta,\dot{\theta}) = \begin{bmatrix} 0 & -b_2\sin\theta_1\dot{\theta}_1 & -b_3\sin\theta_2\dot{\theta}_2 \\ 0 & 0 & -b_5\sin(\theta_1-\theta_2)\dot{\theta}_2 \\ 0 & b_5\sin(\theta_1-\theta_2)\dot{\theta}_1 & 0 \end{bmatrix},$$

$$\mathbf{G}(\theta) = \begin{bmatrix} 0 \\ -b_2g\sin\theta_1 \\ -b_3g\sin\theta_2 \end{bmatrix}, \quad \mathbf{H} = \begin{bmatrix} 1 \\ 0 \\ 0 \end{bmatrix}.$$

The constants b_1 through b_6 are introduced to simplify the representation of the system matrices. They are defined as $b_1 = m_0+m_1+m_2$, $b_2 = m_1l_1+m_2L_1$, $b_3 = m_2l_2$, $b_4 = m_1l_1^2 + J_1 + m_2L_1^2$, $b_5 = m_2L_1l_2$, and $b_6 = m_2l_2^2 + J_2$.

To facilitate controller design, the Lagrange equations of motion in Eq. (9) are reformulated as a sixth-order system of ordinary differential equations by introducing the state vector $\theta \in \mathbb{R}^6$, $\theta = \begin{bmatrix}\theta_0 & \theta_1 & \theta_2 & \dot{\theta}_0 & \dot{\theta}_1 & \dot{\theta}_2\end{bmatrix}^T$. Letting $\mathbf{x} = \theta$ and neglecting the explicit dependence of the system matrices on the generalized coordinates and their derivatives, the dynamics can be written in the compact state–space form

$$\dot{\mathbf{x}} = \begin{bmatrix} \mathbf{0} & \mathbf{I} \\ -\mathbf{D}^{-1}\mathbf{C} & \mathbf{0} \end{bmatrix}\mathbf{x} + \begin{bmatrix} \mathbf{0} \\ -\mathbf{D}^{-1}\mathbf{G} \end{bmatrix} + \begin{bmatrix} \mathbf{0} \\ \mathbf{D}^{-1}\mathbf{H} \end{bmatrix}u. \quad (10)$$

Because the dynamics of the DIPC are inherently nonlinear, a first–order linearization about the equilibrium point $\theta = 0$ is adopted to enable the application of optimal control methods such as LQR. The system admits two equilibria: a stable configuration with the first and second pendulums hanging downward ($\theta_1 = \theta_2 = 180°$) and an unstable configuration with both pendulums aligned vertically upward against gravity ($\theta_1 = \theta_2 = 0°$). Linearization about the unstable equilibrium yields the standard state–space model

$$\begin{aligned} \dot{\mathbf{x}} &= \mathbf{A}\mathbf{x} + \mathbf{B}u, \\ \mathbf{y} &= \mathbf{C}\mathbf{x} + \mathbf{D}u, \end{aligned} \quad (11)$$

with

$$\mathbf{A} = \begin{bmatrix} \mathbf{0} & \mathbf{I} \\ -\mathbf{D}(\mathbf{0})^{-1}\dfrac{\partial\mathbf{G}(\mathbf{0})}{\partial\theta} & \mathbf{0} \end{bmatrix}, \quad \mathbf{B} = \begin{bmatrix} \mathbf{0} \\ \mathbf{D}(\mathbf{0})^{-1}\mathbf{H} \end{bmatrix},$$

$$\mathbf{C} = \mathrm{diag}(\mathbf{I}_6), \quad \mathbf{D} = \mathbf{0}.$$

3. Controller design

3.1 Fuzzy Linear Quadratic Regulator

The design of the FLQR begins with the formulation of the underlying LQR controller. In this framework, the weighting matrices are defined to balance state performance and control effort. Specifically, the state weighting matrix $\mathbf{Q} \in \mathbb{R}^{n\times n}$ penalizes deviations of the state variables, where n corresponds to the order of the linearized system, while the control weighting matrix $\mathbf{R} \in \mathbb{R}^{m\times m}$ penalizes the control input, with m denoting the number of inputs. For the DIPC system, the model dimension is $n = 6$ and the control dimension is $m = 1$, reflecting six state variables and a single control force applied to the cart.

The weighting matrices $\mathbf{Q}$ and $\mathbf{R}$ are defined as:

$$\mathbf{Q} = \begin{bmatrix} Q_1 & 0 & 0 & 0 & 0 & 0 \\ 0 & Q_2 & 0 & 0 & 0 & 0 \\ 0 & 0 & Q_3 & 0 & 0 & 0 \\ 0 & 0 & 0 & Q_4 & 0 & 0 \\ 0 & 0 & 0 & 0 & Q_5 & 0 \\ 0 & 0 & 0 & 0 & 0 & Q_6 \end{bmatrix}, \quad \mathbf{R} = [R_1]$$

The resulting control law generated by the LQR is given by:

$$u = -\mathbf{K}\mathbf{x} \quad (12)$$

where the gain matrix $\mathbf{K} \in \mathbb{R}^{m\times n}$ is computed as: $\mathbf{K} = R^{-1}B^\top P$. Here, $\mathbf{P} \in \mathbb{R}^{n\times n}$ is the unique, positive definite solution of the Riccati Equation:

$$A^\top P + PA - PBR^{-1}B^\top P + Q = 0 \quad (13)$$

Fuzzy Logic Controllers (FLCs) operate through three main stages: input, processing, and output. Sensor signals are first pre-processed and mapped to membership functions to generate fuzzy inputs. These inputs trigger a set of predefined rules in the processing stage, and the fuzzy results are then defuzzified into crisp outputs. In this work, the FLC approach is integrated with the optimal control method LQR to form a hybrid controller. The FLC models are implemented in Simulink using fusion functions, each receiving six inputs, six DIP status variables, and producing two outputs: the error e and the derivative of the error ec. Figure 2 illustrates the resulting closed-loop system.

With a reference input of zero and the initial values of the two pendulums set to $\frac{\pi}{6}$ radians, the parameters K_E, K_{EC}, and

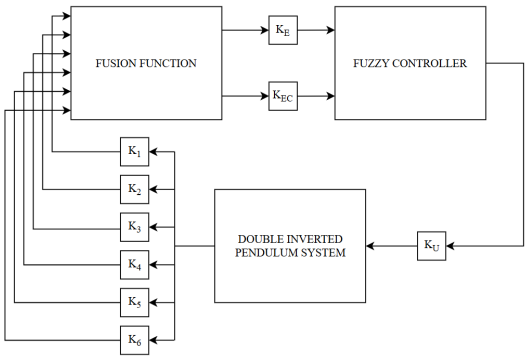

Figure 2: Closed-loop DIPC system

E \ EC	NB	NM	NS	ZE	PS	PM	PB
NB	NB	NB	NB	NM	NM	NS	ZE
NM	NB	NB	NM	NM	NS	ZE	PS
NS	NB	NM	NM	NS	ZE	PS	PM
ZE	NM	NM	NS	ZE	PS	PM	PM
PS	NM	NS	ZE	PS	PM	PM	PB
PM	NS	ZE	PS	PM	PM	PB	PB
PB	ZE	PS	PM	PM	PB	PB	PB

Table 1: The Fuzzy rules

K_U were tuned through trial-and-error testing. Under these conditions, the selected values were $K_E = 3$, $K_{EC} = 0.3$, and $K_U = 32$.

For the rule base, seven categorical variables were used: (i) NB—Negative Big, (ii) NM—Negative Medium, (iii) NS—Negative Small, (iv) ZE—Zero, (v) PS—Positive Small, (vi) PM—Positive Medium, and (vii) PB—Positive Big. These categories correspond to the seven fuzzy sets applied to both inputs and outputs. The complete set of rules is presented in Table 1.

Figure 3 illustrates the control surface of the fuzzy controller, showing the relationship between the error (e), the derivative of error ($\dot{e}$, denoted as EC), and the control output (u). As observed, the surface exhibits a smooth and continuous transition, indicating that the controller provides gradual and stable control actions over the entire operating range. The surface indicates appropriate rule tuning, with strong control actions at large errors and near-zero output around equilibrium.

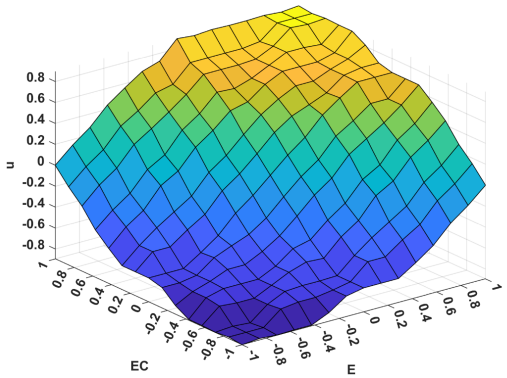

Figure 3: The FLC surface

To compute the fusion function, we used the following values for the matrix **K**:

$$\mathbf{K} = [K_{\theta_0}, K_{\theta_1}, K_{\theta_2}, K'_{\theta_0}, K'_{\theta_1}, K'_{\theta_2}]$$

These values in the matrix **K** are calculated from the previously simulated and optimized LQR control model. Subsequently, the fusion function is computed using the formula outlined below, with the values from matrix **K** being applied to achieve optimal performance in combining the control signals.

$$F_{fus}(x) = \begin{bmatrix} \frac{K_{\theta_0}}{K_{\theta_2}} & \frac{K_{\theta_1}}{K_{\theta_2}} & \frac{K_{\theta_2}}{K_{\theta_2}} & 0 & 0 & 0 \\ 0 & 0 & 0 & \frac{K_{\theta'_0}}{K_{\theta'_2}} & \frac{K_{\theta'_1}}{K_{\theta'_2}} & \frac{K_{\theta'_2}}{K_{\theta'_2}} \end{bmatrix} \begin{bmatrix} \theta_0 \\ \theta_1 \\ \theta_2 \\ \theta'_0 \\ \theta'_1 \\ \theta'_2 \end{bmatrix} \tag{14}$$

(14)

3.2 Fuzzy Linear Quadratic Gaussian controller

The combined state-space model is formulated as:

$$\begin{bmatrix} \dot{x} \\ \dot{\varepsilon} \end{bmatrix} = \begin{bmatrix} A - BK & BK \\ 0 & A - K_f C \end{bmatrix} \begin{bmatrix} x \\ \varepsilon \end{bmatrix} + \begin{bmatrix} 1 & 0 \\ 1 & -K_f \end{bmatrix} \begin{bmatrix} W_d \\ W_n \end{bmatrix} \tag{15}$$

The structure of the Fuzzy Linear Quadratic Gaussian (FLQG) controller is developed by integrating the LQG and FLQR approaches. In practical applications, it is often not feasible to directly measure all the state variables of the system. However, if the system is observable, the unmeasured states can be estimated from the available output data. Furthermore, when the measurement data are corrupted by noise, employing an observer to estimate the system states becomes a rational and widely adopted solution.

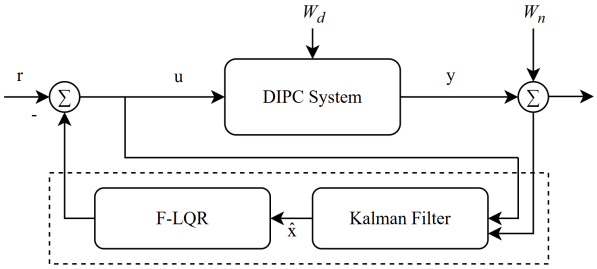

Figure 4: Block diagram of the FLQG.

The FLQG structure is established by incorporating a KF into the FLQR control system, as shown in Figure 4. The KF is essential when the state variables required by the FLQR controller cannot be directly measured and must instead be estimated. It performs this estimation using the input signals of the DIPC system together with the experimentally measured outputs, and the resulting estimated states are then supplied to the FLQR controller.

3.3 High gain observer

In modern control systems, especially for highly nonlinear systems like the double inverted pendulum on a cart, it is often impractical to measure all state variables directly. Typically, only the cart position and pendulum angles can be measured, while the corresponding velocities are either difficult to measure or highly sensitive to noise when estimated via numerical differentiation. Therefore, a state observer becomes an essential component in the control architecture. The HGO is a prominent state estimation technique due to its ability to provide fast and accurate estimates, particularly effective when the system model is well-known and measurement noise is limited. With its simple structure, the HGO is easy to implement in both simulations and real-time systems, serving as a practical

bridge that enables controllers such as LQR to operate under partial state measurement conditions.

In the previous sections, we introduced the LQG and FLQG controllers for the double-inverted pendulum on a cart. Both controllers employ the KF to estimate the state of the system under noisy conditions. However, implementing the KF requires full-state measurements of the system. In practice, obtaining complete state measurements is often infeasible due to sensor limitations or measurement noise. To overcome these challenges, we propose incorporating a state estimation technique: the HGO as seen in Figure 5.

In the case of a double inverted pendulum on a cart, the observer is designed to estimate the cart velocity and the angular velocities of both pendulums using the cart position and the two pendulum angles as input. The measurable inputs of the system are the cart position x_1, the angle of pendulum 1 (x_2), and the angle of pendulum 2 (x_3). Based on these measured variables, the High-Gain Observer is designed to estimate the unmeasurable states, namely the cart velocity $\dot{x}_1$, the angular velocity of pendulum 1 ($\dot{x}_2$), and the angular velocity of pendulum 2 ($\dot{x}_3$).

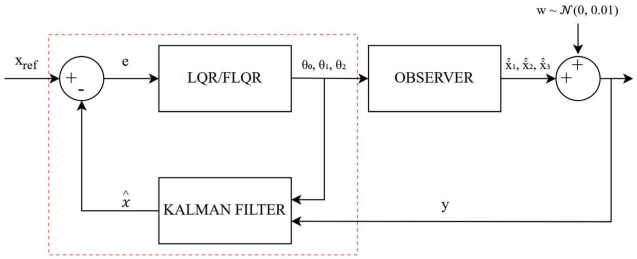

Figure 5: LQG and FLQG Observer Diagram

The observer is designed using an extended state model with a 3-stage integrator structure:

$$\hat{x} = \begin{bmatrix} \hat{x}_1 & \hat{x}_2 & \hat{x}_3 & \hat{x}_4 & \hat{x}_5 & \hat{x}_6 \end{bmatrix}^T$$

where:

$$\hat{x}_1 \approx x_1, \quad \hat{x}_2 \approx x_2, \quad \hat{x}_3 \approx x_3$$

are estimates of the measured states, and:

$$\hat{x}_4 \approx \dot{x}_1, \quad \hat{x}_5 \approx \dot{x}_2, \quad \hat{x}_6 \approx \dot{x}_3$$

are the estimated velocities. The observation errors are defined as the differences between the measured and estimated states.

$$e_1 = \hat{x}_1 - x_1, \quad e_2 = \hat{x}_2 - x_2, \quad e_3 = \hat{x}_3 - x_3$$

The observer differential equations are given by:

$$\dot{\hat{x}}_1 = \hat{x}_4 - \frac{\alpha_2}{\varepsilon} e_1$$
$$\dot{\hat{x}}_2 = \hat{x}_5 - \frac{\alpha_2}{\varepsilon} e_2$$
$$\dot{\hat{x}}_3 = \hat{x}_6 - \frac{\alpha_2}{\varepsilon} e_3$$
$$\dot{\hat{x}}_4 = -\frac{\alpha_1}{\varepsilon^2} e_1$$
$$\dot{\hat{x}}_5 = -\frac{\alpha_1}{\varepsilon^2} e_2$$
$$\dot{\hat{x}}_6 = -\frac{\alpha_1}{\varepsilon^2} e_3$$

where: α_1, α_2 are high-gain coefficients. ε is a small positive parameter (typically $\varepsilon \ll 1$) used to accelerate convergence.

Remark 1. *In the design of the High-Gain Observer (HGO), the parameters α_1 and α_2 are introduced to tune the convergence speed of the estimation error. The HGO structure is formulated as an extended three-layer integrator model, in which $\frac{\alpha_1}{\varepsilon^2}$ determines the convergence rate of the error between the measured and estimated states, and $\frac{\alpha_2}{\varepsilon}$ controls the amplification of the error signal in the first layer, directly affecting sensitivity to measurement noise. After scanning the parameter ranges:*

$$\alpha_1 \in [5, 12], \qquad \alpha_2 \in [3, 8],$$

The selected values are:

$$\alpha_1 = 9, \qquad \alpha_2 = 6.$$

If these parameters are chosen too large, the estimated states may become noisy and affect controller stability; conversely, if they are too small, the estimation error increases and degrades the performance of the FLQG controller.

4. Simulation Results

In this part, the developed controllers, i.e., the FLQR and the FLQG, are modeled for the stabilization of the DIPC. The system is evaluated using the parameters $m_0 = 0.8$ kg, $m_1 = 0.5$ kg, $m_2 = 0.3$ kg, $L_1 = 0.3$ m, $L_2 = 0.3$ m, $J_1 = 0.015\ \text{kg}\cdot\text{m}^2$, $J_2 = 0.009\ \text{kg}\cdot\text{m}^2$, and $g = 9.8\ \text{m/s}^2$. The initial conditions are set to $\theta_0 = 0$ m, $\theta_1 = \pi/6$ rad, and $\theta_2 = \pi/6$ rad. To enable state estimation, the high-gain observer is designed with parameters $\alpha_1 = 9$, $\alpha_2 = 6$, and $\varepsilon = 0.01$.

4.1 The ideal case

The performance of the FLQR controller was evaluated through simulation under ideal conditions, in which all output variables were assumed to be measurable, and no measurement noise was present. The simulation was conducted using the gain matrix $\mathbf{K} = [3.16,\ -125.95,\ 145.03,\ 4.84,\ -1.08,\ 12.63]$ and the initial state vector $\mathbf{x}^T = [0,\ \pi/6,\ \pi/6,\ 0,\ 0,\ 0]$.

As shown in Fig. 6, the FLQR controller effectively regulates the system states to their desired equilibrium points. In particular, the pendulum angles θ_1 and θ_2 are stabilized, while the cart position, which is subject to an external disturbance that displaces it by 0.5 m every 40 seconds, is successfully controlled and returned to the reference position. The figure further illustrates the evolution of the angular signals θ_0, θ_1, and θ_2 under the FLQR strategy. The simulation results demonstrate that the FLQR controller achieves strong control performance and exhibits high robustness against disturbances. Specifically, it enhances dynamic performance measures such as settling time (T_s), overshoot (PO), steady-state error (E_{ss}), and root mean square error (RMSE). Moreover, the controller consistently maintains system stability under external disturbances, with a detailed quantitative comparison of performance indices provided in Table 2.

4.2 The realistic case: Noise and external disturbance

The simulation results obtained from the FLQR controller were conducted under the ideal case, where no measurement

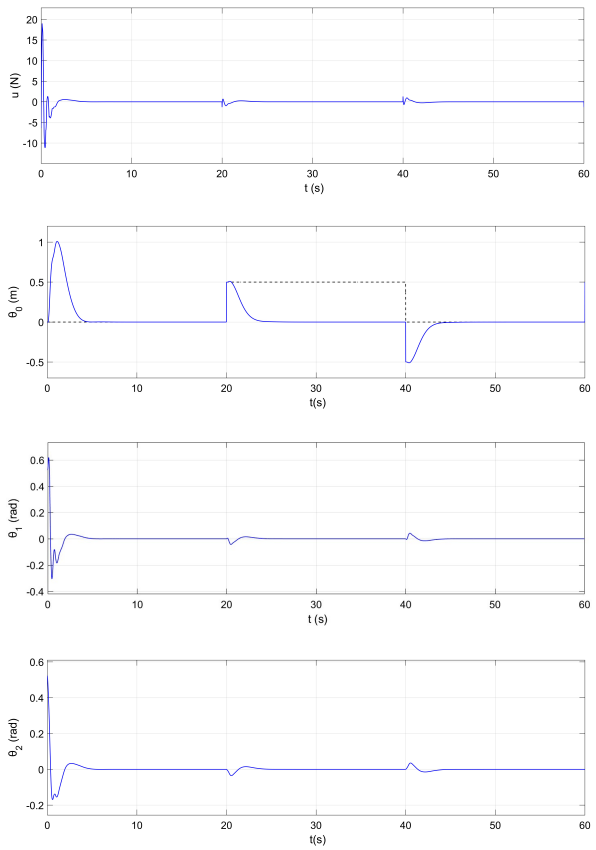

Figure 6: The angle signals (u, θ_0, θ_1, θ_2) with FLQR controller.

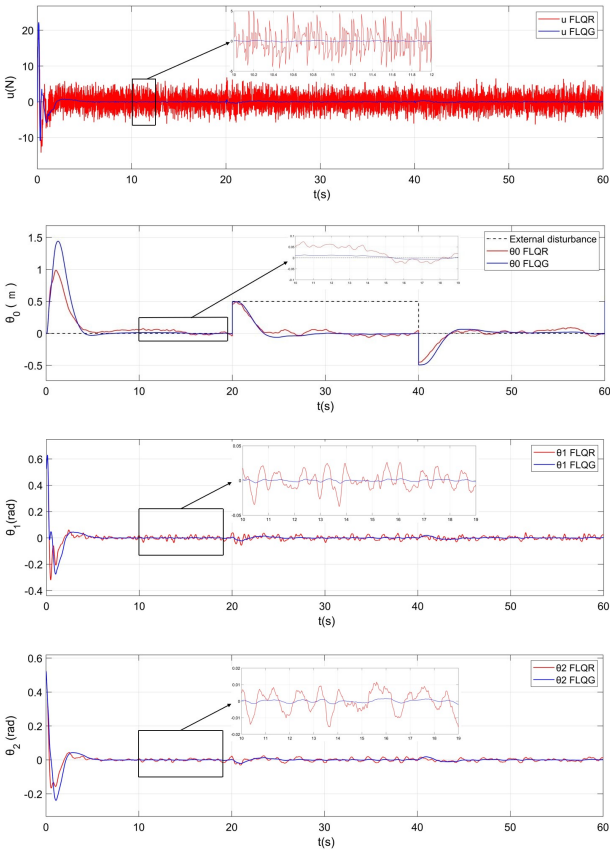

Figure 7: The angle signals (u, θ_0, θ_1, θ_2) with FLQR and FLQG controllers.

Table 2: Quantitative comparison of performance of LQR and FLQR controllers under external disturbance.

Controller	Joints			
	Parameters	Position car (θ_0)	First Link (θ_1)	Second Link (θ_2)
LQR	T_s	5.39 s	3.8 s	3.8 s
	PO	1.13 m	0.6 rad	0.52 rad
	E_{ss}	0.001	0.001	0.001
	RMSE	0.19	0.057	0.05
FLQR	T_s	4 s	3.6 s	3.6 s
	PO	1.01 m	0.61 rad	0.52 rad
	E_{ss}	0.001	0.001	0.001
	RMSE	0.17	0.055	0.046

noise was present, and all state variables were assumed to be measurable. However, such conditions do not fully reflect the actual implementation in a physical system. In practice, the system is often affected by noise, and it is not always possible to measure all variables, such as velocity and angular velocity.

To better approximate real-world conditions, the realistic case was considered by introducing white noise with different signal-to-noise ratios (SNRs) into the system during the simulation. At the same time, an HGO is employed to estimate the three velocity variables θ_0', θ_1', and θ_2' from the measured position variables θ_0, θ_1, and θ_2.

The performance of the FLQR controller was then evaluated under these noisy conditions, while the FLQG controller demonstrated the capability to estimate the system states and maintain effective performance even in the presence of measurement noise.

Using the same parameters of the DIPC model and the initial condition vector described earlier, the results indicate that the FLQG controller provides effective disturbance rejection and preserves system stability throughout the simulation.

The key distinction between the FLQR and FLQG controllers lies in their ability to handle disturbances. While the FLQR controller lacks explicit disturbance filtering mechanisms, the FLQG controller integrates algorithms designed to mitigate the impact of external and measurement disturbances. As illustrated in Fig. 7, disturbances noticeably affect the system output under FLQR control, whereas this effect is significantly reduced when the FLQG controller is applied. A quantitative comparison of performance indices, including settling time (T_s), overshoot (PO), steady-state error (E_{ss}), and root mean square error (RMSE), is provided in Table 3 under external and combined disturbance conditions.

Table 3: Quantitative Comparison of Performance of LQG and FLQG Controllers under Noise and External Disturbance.

Controller	Joints			
	Parameters	Position car (θ_0)	First Link (θ_1)	Second Link (θ_2)
LQG	T_s	6.3 s	4.4 s	4.4 s
	PO	1.8 m	0.61 rad	0.52 rad
	E_{ss}	0.015	0.0035	0.004
	RMSE	0.29	0.065	0.059
FLQG	T_s	5.7 s	4.27 s	4.3 s
	PO	1.44 m	0.62 rad	0.52 rad
	E_{ss}	0.01	0.003	0.003
	RMSE	0.23	0.06	0.051

5. Conclusion

This work proposed and evaluated hybrid control strategies for stabilizing the DIPC. By integrating fuzzy logic with optimal control, the FLQR and the FLQG controllers have been

developed, with an HGO added to estimate unmeasured velocity states from measurable positions and angles. Simulation studies under both ideal and realistic conditions demonstrated that, while FLQR performs well in noise-free scenarios, the FLQG with HGO consistently achieves faster settling time, reduced overshoot, lower steady-state error. These results confirm the effectiveness and practicality of combining fuzzy logic, optimal control, and observer-based state estimation for robust control of nonlinear and underactuated systems.

Acknowledgement

This research is funded by Hanoi University of Science and Technology (HUST) under project number T2024-TD-015.

References

[1] B. He, S. Wang, and Y. Liu, "Underactuated robotics: A review," *International Journal of Advanced Robotic Systems*, vol. 16, no. 4, p. 1 729 881 419 862 164, 2019. DOI: 10.1177/1729881419862.

[2] H. N. Le, P. V. Dang, A.-D. Pham, and N. T. Vo, "System identifications of a 2dof pendulum controlled by qube-servo and its unwanted oscillation factors," *Archive of Mechanical Engineering*, pp. 435–450, 2020.

[3] A.-D. Pham and H.-J. Ahn, "Evaluation of input shaping methods for the nonlinear vibration system using a furuta pendulum," *Korean Soc. Precis. Eng*, 2020. DOI: 10.7736/JKSPE.020.056.

[4] M. S. Daksh and P. Mishra, "A feedback-assisted inverse neural network controller for cart-mounted inverted pendulum," *Applied Computational Intelligence and Soft Computing*, vol. 2025, no. 1, p. 4 873 425, 2025. DOI: 10.1155/acis/4873425.

[5] A.-T. Nguyen, A. Dequidt, V.-A. Nguyen, L. Vermeiren, and M. Dambrine, "Fuzzy descriptor tracking control with guaranteed L_∞ error-bound for robot manipulators," *Transactions of the Institute of Measurement and Control*, vol. 43, no. 6, pp. 1404–1415, 2021. DOI: 10.1177/014233122097.

[6] P. Biswal and P. K. Mohanty, "Development of quadruped walking robots: A review," *Ain Shams Engineering Journal*, vol. 12, no. 2, pp. 2017–2031, 2021. DOI: 10.1016/j.asej.2020.11.005.

[7] J. Chen, N. He, Z. Xu, M. Dou, and L. He, "Design and implementation of a novel two-wheeled composite self-balancing robot for stationary operations in unknown terrain," *IEEE Access*, 2025. DOI: 10.1109/ACCESS.2025.3569325.

[8] Y.-c. Xie, H. Huang, Y. Hu, and G.-q. Zhang, "Applications of advanced control methods in spacecrafts: Progress, challenges, and future prospects," *Frontiers of Information Technology & Electronic Engineering*, vol. 17, no. 9, pp. 841–861, 2016. DOI: 10.1631/FITEE.1601063.

[9] H. Maghfiroh, M. Nizam, M. Anwar, and A. Ma'Arif, "Improved lqr control using pso optimization and kalman filter estimator," *IEEE Access*, vol. 10, pp. 18 330–18 337, 2022. DOI: 10.1109/ACCESS.2022.3149951.

[10] N. T. Vo, A.-D. Pham, and D. M. T. Nguyen, "Hierarchical sliding mode control with oscillation compensation for low-cost inverted pendulum systems using hardware-in-loop," *Archive of Mechanical Engineering*, pp. 31–55, 2025.

[11] D. Wang, H. He, and D. Liu, "Intelligent optimal control with critic learning for a nonlinear overhead crane system," *IEEE Transactions on Industrial Informatics*, vol. 14, no. 7, pp. 2932–2940, 2017. DOI: 10.1109/TII.2017.2771256.

[12] H.-P. Nguyen, N.-T. Bui, et al., "Tracking control based on takagi-sugeno fuzzy descriptor model for overhead crane combined with input shaping," *IEEE Access*, 2024. DOI: 10.1109/ACCESS.2024.3456815.

[13] Y. Gao, Z. Zhang, P. Huang, and Y. Wu, "Adaptive tracking controller for fas with state constraints and its application to underactuated overhead cranes: Design and experiment," *IEEE Transactions on Industrial Electronics*, 2024. DOI: 10.1109/TIE.2024.3488372.

[14] T.-V.-A. Nguyen, Q.-T. Dao, and N.-T. Bui, "Optimized fuzzy logic and sliding mode control for stability and disturbance rejection in rotary inverted pendulum," *Scientific Reports*, vol. 14, no. 1, p. 31 116, 2024. DOI: 10.1038/s41598-024-82471-y.

[15] D. Vázquez and M. Bernal, "Lmi-based nonlinear control via implicit lyapunov function for finite-time stabilization," *IEEE Transactions on Automatic Control*, 2025. DOI: 10.1109/TAC.2025.3597890.

[16] B.-T. Dong and T.-V.-A. Nguyen, "Simplified lmi conditions for takagi-sugeno fuzzy observer design with unmeasured premise variables," *International Journal of Fuzzy Systems*, vol. 27, no. 3, pp. 762–773, 2025. DOI: 10.1007/s40815-024-01803-2.

[17] R. Tang, P. Shi, X. Yang, G. Wen, and L. Shi, "Finite-time synchronization of coupled fractional-order systems via intermittent it-2 fuzzy control," *IEEE Transactions on Systems, Man, and Cybernetics: Systems*, 2025. DOI: 10.1109/TSMC.2024.3518513.

[18] V.-A. Nguyen, L. Vermeiren, A. Dequidt, A.-T. Nguyen, M. Dambrine, and L. Cung, "Takagi-sugeno fuzzy descriptor approach for trajectory control of a 2-dof serial manipulator," in *2018 13th IEEE Conference on Industrial Electronics and Applications (ICIEA)*, IEEE, 2018, pp. 1284–1289. DOI: 10.1109/ICIEA.2018.8397907.

[19] B. Bekkar and K. Ferkous, "Design of online fuzzy tuning lqr controller applied to rotary single inverted pendulum: Experimental validation," *Arabian Journal for Science and Engineering*, vol. 48, no. 5, pp. 6957–6972, 2023. DOI: 10.1007/s13369-022-06921-3.

[20] K. C. Veluvolu, M. Defoort, and Y. C. Soh, "High-gain observer with sliding mode for nonlinear state estimation and fault reconstruction," *Journal of the Franklin Institute*, vol. 351, no. 4, pp. 1995–2014, 2014. DOI: 10.1016/j.jfranklin.2012.12.018.